Frequency synchronization of a high-order multi-converter system

Frequency Synchronization of a High-Order Multiconverter System

Taouba Jouini, *Member, IEEE*, and Zhiyong Sun, *Member, IEEE*

***Abstract*—We investigate the frequency stability of a high-order multi-converter system. For this, we identify its symmetry (i.e., rotational invariance) generated by a static angle shift and rotation of ac signals. We characterize the synchronous steady-state set, primarily determined by the steady-state angles, and dc power input. Based on eigenvalue conditions of its Jacobian matrix, we show asymptotic stability of the multi-converter system in a neighborhood of the frequency synchronous steady-state set by applying the center manifold theory. We guarantee the Jacobian's eigenvalue condition via an explicit approach that requires sufficient damping on the dc and ac side. Finally, we demonstrate our results based on a numerical example involving a network of dc/ac converters.**

***Index Terms*—Dc/ac converters, Lyapunov methods, nonlinear network analysis, power system stability.**

I. Introduction

ELECTRICITY production is one of the largest sources of greenhouse gas emissions in the world. Carbon-free electricity will be critical for keeping the average global temperature within the United Nation's target and avoiding the worst effects of climate change [1]. Prompted by these environmental concerns, the electrical grid has witnessed a major shift in power generation from conventional (coal, oil) into renewable (wind, solar) resources. The massive deployment of distributed, renewable generation had an elementary effect on its operation via power electronics converters interfacing the grid, deemed as game changers of the conventional analysis methods of power system stability and control.

Literature Review: Modeling and stability analysis in power system networks is conducted as a matter of perspective from two different angles. First, network perspective suggests an *up to bottom* approach, where dc/ac converter dynamics are regarded as controllable voltage sources and voltage control is directly accessible. The most prominent example is droop control that leads to the study of second-order pendulum dynamics, emulating the swing equation of synchronous machines [2], which resembles the celebrated Kuramoto-oscillator [3]. The analogy drawn between the two models has motivated a vast body of literature that harnesses the results available for synchronization via Kuramoto oscillators to analyze frequency stability in power systems. Second, a *bottom to up* approach derives dc/ac converter models from first-order principles, where their governing dynamics are inferred from the circuitry of the dc and ac side and the intermediate switching block, which can structurally match that of synchronous machines. Recently, the matching control has been proposed in [4] as a promising control strategy, which achieves a structural equivalence of the two models and endows the closed-loop system with advantageous features (droop properties, power sharing, etc.). By augmenting the system dynamics with a virtual angle, the frequency is set to be proportional to dc capacitor voltage deviations, constituting a measure of power imbalance in the grid. This leads to the derivation of higher order models that describe a network of coupled dc/ac converters on high-order nonlinear manifolds.

Similar to the physical world, where the laws governing interactions in a set of particles are invariant with respect to static translations and rotations of the whole rigid body [5], power system trajectories are invariant under a static shift in their angles, or said to possess a *rotational invariance*. The symmetry of the vector field describing the power system dynamics indicates the existence of a continuum of steady states for the multi-converter (with suitable control that induces/preserves angle symmetry) or multi-machine dynamics. In particular, the rotational invariance is the topological consequence of the absence of a reference frame or absolute angle in power systems and regarded thus far as a fundamental obstacle for defining suitable error coordinates for the stability analysis. To alleviate this, a common approach is to perform transformations either resulting from projecting into the orthogonal complement, if the steady-state set is a linear subspace [6], or grounding a node [7], where classical stability tools, such as the Lyapunov direct method, can be deployed.

To analyze power system stability, different conditions have been proposed. In [4] and [8], sufficient stability conditions are obtained for a single-machine/converter connected to a load. In [3], a sufficient algebraic stability condition connects the synchronization of power systems with network connectivity and power system parameters. Although these conditions give qualitative insights into the sensitivities influencing stability, they usually require strong and often unrealistic assumptions.

Manuscript received July 26, 2021; accepted October 4, 2021. Date of publication November 16, 2021; date of current version June 20, 2022. This work was supported in part by the European Research Council (ERC) under the European Union's Horizon 2020 research and innovation program under Grant 834142, in part by the European Union's Horizon 2020 research and innovation program under Grant 691800, and in part by ETH Zürich funds. Recommended by Associate Editor Joshua A. Taylor. *(Corresponding author: Taouba Jouini.)*

Taouba Jouini is with the Department of Automatic Control, LTH, Lund University, 22363 Lund, Sweden (e-mail: taouba.jouini@control.lth.se).

Zhiyong Sun is with the Department of Electrical Engineering, Eindhoven University of Technology, 5612 AZ Eindhoven, The Netherlands (e-mail: sun.zhiyong.cn@gmail.com).

Digital Object Identifier 10.1109/TCNS.2021.3128493

For example, the underlying models are of reduced order (mostly first or second order) [3], [9]. Reduced-order systems, where one infers stability of the whole system from looking at only a subset of variables, are not a truthful representation of the full-order dynamics if important assumptions are not met [10]. Some stability conditions are valid only in radial networks [6]. Moreover, implicit conditions, e.g., based on semi-definite programming are not very insightful [11].

Contributions: In this work, we ask in essence two fundamental questions: 1) Under mild assumptions on input feasibility, how can we describe the behavior of the steady-state trajectories of the nonlinear power system in closed-loop with a suitable control that induces/preserves the symmetry, e.g., the matching control [4], [12]? 2) Based on the properties of the steady-state manifold, can we ensure local stability, i.e., local frequency synchronization?

To answer the first question, we study the behavior of the steady-state set. For this, we derive a steady-state map, which embeds known steady-state angles into the dc power inputs to the converters as a function of the network topology and converter parameters. We show that the steady-state angles fully describe the steady-state behavior and determine all other states. The steady-state map depends on network topology, which is known to play a crucial role in the synchronization of power systems [5], [6]. Since the vector field exhibits symmetry with respect to translation and rotation actions, i.e., under a shift in all angles and a rotation in all ac signals, the steady-state manifold inherits the same property and every steady-state trajectory is invariant under the same actions. This allows us to define a frequency synchronous steady-state set generated under these actions.

We address the second question by showing asymptotic stability of the nonlinear trajectories confined to a neighborhood of the frequency synchronous steady-state set. For this, we study the stability of the nonlinear dynamics as a direct application of the center manifold theory to the multi-converter power system. We assume that the eigenvalues of the Jacobian evaluated at a frequency synchronous steady state can be split into one mode at zero and the rest in the open-left half-plane. Then, we can decompose the nonlinear system into two interconnected subsystems, whose dynamics are dictated by zero and Hurwitz matrices, respectively. This allows to define a center manifold upon modal transformation, where we use the reduction principle [13, p.195] to deduce the stability of the trajectories of the multi-converter system from the dynamics evolving on the center manifold. The point-wise application of the center manifold theory allows to construct a neighborhood of the frequency synchronous steady-state set and thereby shows its local asymptotic stability.

To satisfy the Jacobian eigenvalue condition in an explicit way, we study the linearized system trajectories and pursue a parametric linear stability analysis approach at a frequency synchronous steady state. Toward this, we develop a novel stability analysis for a class of partitioned linear systems characterized by a stable subsystem and 1-D invariant subspace. We propose a new class of Lyapunov functions characterized by an oblique projection onto the complement of the Jacobian zero eigenspace, where the inner product is taken with respect to a matrix to be chosen as the solution to Lyapunov and $\mathcal{H}_\infty-$algebraic Riccati equations (ARE). For the multi-source power system model, we arrive at explicit stability conditions that depend only on the converter's parameters and steady-state values. In accordance with other works, our conditions require sufficient dc and ac side damping.

Paper Organization This article unfurls as follows: Section II presents the model setup based on a high-order power system model. Section III characterizes the frequency synchronous steady-state set and feasible inputs. Section IV studies local asymptotic stability of the nonlinear power system using center manifold theory. Section V proposes one approach to satisfy the Jacobian's eigenvalue condition. Section VI exemplifies our theory via simulations in two test cases. Finally, Section VII concludes this article.

Notation: Define an undirected graph $\mathbb{G} = (\mathcal{V}, \mathcal{E})$, where $\mathcal{V}$ is the set of nodes with $|\mathcal{V}| = n$ and $\mathcal{E} \subseteq \mathcal{V} \times \mathcal{V}$ is the set of interconnected edges with $|\mathcal{E}| = m$. We assume that the topology specified by $\mathcal{E}$ is arbitrary and define the map $\mathcal{E} \to \mathcal{V}$, which associates each oriented edge $e_{ij} = (i, j) \in \mathcal{E}$ to an element from the subset $\mathcal{I} = \{-1, 0, 1\}^{|\mathcal{V}|}$, resulting in the incidence matrix $\mathcal{B} \in \mathbb{R}^{n\times m}$. We denote the identity matrix by $I = \begin{bmatrix} 1 & 0 \\ 0 & 1 \end{bmatrix}$, and $\mathbf{I}$ the identity matrix of suitable dimension $p \in \mathbb{N}$ and $\mathbf{J} = \mathbf{I} \otimes J_2$ with $J_2 = \begin{bmatrix} 0 & -1 \\ 1 & 0 \end{bmatrix}$. We define the rotation matrix $R(\gamma) = \begin{bmatrix} \cos(\gamma) & -\sin(\gamma) \\ \sin(\gamma) & \cos(\gamma) \end{bmatrix}$ and $\mathbf{R}(\gamma) = \mathbf{I} \otimes R(\gamma)$. Let $\mathrm{diag}(v)$ denote a diagonal matrix, whose diagonals are elements of the vector v and $\mathrm{Rot}(\gamma) = \mathrm{diag}(r(\gamma_k)),\ k = 1 \dots n$, with $r(\gamma_k) = [-\sin(\gamma_k)\ \cos(\gamma_k)]^\top$. Let $\mathbb{1}_n$ be the $n-$dimensional vector with all entries being one and $\mathbb{T}^n = \mathbb{S}^1 \times \cdots \times \mathbb{S}^1$ is the $n-$dimensional torus. We denote by $d(\cdot, \cdot)$ a distance metric. Given a set $\mathcal{A} \subseteq \mathbb{R}^n$, then $d(z, \mathcal{A}) = \inf_{x\in\mathcal{A}} d(z, x)$ and $T_z\,\mathcal{A}$ is the tangent space of $\mathcal{A}$ at z. Given a vector $v \in \mathbb{R}^n$, we denote by $v^\perp$ its orthogonal complement, v_k its k-th entry. For a matrix A, let $\|A\|_2 = \overline{\sigma}(A)$ denote its induced two-norm and $\overline{\sigma}(A)$ denote its maximum singular value. Given dynamical system $\dot{x} = f(x)$, $x(0) = x_0$, let $J_f(x^*) = \frac{\partial f(x)}{\partial x}\big|_{x=x^*}$ be the system Jacobian evaluated at some point $x = x^*$.

II. Modeling and Setup

A. Multisource Power System Dynamics

We start from the following high-order model describing the evolution of the dynamics of $n-$identical three-phase balanced and averaged dc/ac converters interconnected through $m-$identical resistive and inductive lines. An example of the converter circuit diagram is depicted in Fig. 1. Each converter is assumed to be in closed-loop with the matching control, a control strategy that renders its dynamics structurally equivalent to a synchronous machine [4]. At the kth converter input u_k, we assign a sinusoid with constant magnitude $\mu \in]0, 1[$ and frequency $\dot{\gamma}_k \in \mathbb{R}$ given by

$$\dot{\gamma}_k = \eta(v_{\mathrm{dc},k} - v^*_{\mathrm{dc}}) \tag{1a}$$

$$u_k = \mu \begin{bmatrix} -\sin(\gamma_k) \\ \cos(\gamma_k) \end{bmatrix}, \quad k = 1, \dots, n\,. \tag{1b}$$

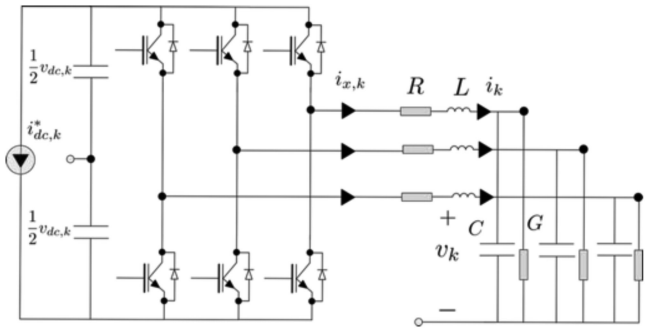

Fig. 1. Circuit diagram of a balanced and averaged three-phase dc/ac converter with $i_{x,k} = \frac{\mu}{2} r^\top(\gamma_k)\, i_k$ and $v_{x,k} = \frac{\mu}{2} r(\gamma_k)\, v_{dc,k}$, see, e.g., [14]. Note that dc conductance is not represented in this diagram.

Here, $\gamma_k \in \mathbb{S}^1$ is the virtual converter angle in the $dq-$frame, after Park transformation, see, e.g., [2], whose angle $\theta_{dq}(t) = \int_0^t \omega^*\, d\tau$ is chosen to rotate at the nominal steady-state frequency $\omega^* > 0$. Moreover, $\eta > 0$ is a control gain defining the slope of the linear map from dc voltage deviation to the oscillator frequency.

The closed-loop converter dynamics are given by the following set of first-order differential equations in the $dq-$frame. For simplicity of notation, we will drop the subscript $dq-$from all ac signals

$$\begin{bmatrix} \dot\gamma_k \\ C_{\rm dc}\dot v_{{\rm dc},k} \\ L\dot i_k \\ C\dot v_k \end{bmatrix} = \begin{bmatrix} \eta(v_{{\rm dc},k} - v^*_{\rm dc}) \\ -K_p(v_{{\rm dc},k} - v^*_{\rm dc}) - \frac{\mu}{2} r(\gamma_k)^\top i_k \\ -(R\,I + L\,\omega^*\,J)\, i_k + \frac{\mu}{2} r(\gamma_k) v_{{\rm dc},k} - v_k \\ -(G\,I + C\,\omega^*\,J)\, v_k + i_k - i_{{\rm net},k} \end{bmatrix} + \begin{bmatrix} 0 \\ i^*_{{\rm dc},k} \\ 0 \\ 0 \end{bmatrix}. \tag{2}$$

Let $v_{{\rm dc},k} \in \mathbb{R}$ denote the voltage across the dc capacitor $C_{\rm dc} > 0$ with nominal value $v^*_{\rm dc}$. The conductance $G_{\rm dc} > 0$, together with the proportional control gain $\hat K_p > 0$, are described by $K_p = G_{\rm dc} + \hat K_p > 0$. This results from designing the controllable current source $i_{{\rm dc},k} = -\hat K_p(v_{{\rm dc},k} - v^*_{\rm dc}) + i^*_{{\rm dc},k}$, where we denote by $i^*_{{\rm dc},k} \in \mathbb{R}$ a constant representing dc side input to the converter. The modulation amplitude μ, feedforward current $i^*_{{\rm dc},k}$ and the control gain $\hat K_p$ are regarded as constants usually determined offline or in outer control loops. See [4] for more details. On the ac side, let $i_k \in \mathbb{R}^2$ be the inductance current and $v_k \in \mathbb{R}^2$ as the output voltage. The filter resistance and inductance are specified by $R > 0$ and $L > 0$, respectively. The capacitor $C > 0$ is set in parallel with the load conductance $G > 0$ to ground and connected to the network via the output current $i_{{\rm net},k} \in \mathbb{R}^2$.

Observe that the closed-loop dc/ac converter dynamics (2) match one-to-one those of a synchronous machine with single-pole pair, non-salient rotor under constant excitation [4]. Thus, all the results derived ahead can conceptually also be applied to synchronous machines.

By lumping the states of $n-$converters and $m-$transmission lines and defining the shunt impedance matrices $Z_R = R\,\mathbf{I} + L\,\omega^*\,\mathbf{J}$, $Z_\ell = R_\ell\,\mathbf{I} + L_\ell\omega^*\,\mathbf{J}$ and shunt admittance matrix $Y_C = G\,\mathbf{I} + C\,\omega^*\,\mathbf{J}$, we obtain the following power system model:

$$\begin{bmatrix} \dot\gamma \\ \dot v_{\rm dc} \\ \dot i \\ \dot v \\ \dot i_\ell \end{bmatrix} = K^{-1} \begin{bmatrix} \eta(v_{\rm dc} - v^*_{\rm dc}\mathbb{1}_n) \\ -K_p(v_{\rm dc} - v^*_{\rm dc}\mathbb{1}_n) - \frac{1}{2}\mu{\rm Rot}(\gamma)^\top i \\ -Z_R\, i + \frac{1}{2}\mu{\rm Rot}(\gamma)\, v_{\rm dc} - v \\ -Y_C\, v + i - \mathbf{B}\, i_\ell \\ -Z_\ell\, i_\ell + \mathbf{B}^\top v \end{bmatrix} + K^{-1} \begin{bmatrix} 0 \\ \mathbf{u} \\ 0 \\ 0 \\ 0 \end{bmatrix} \tag{3}$$

where we define the angle vector $\boldsymbol{\gamma} = [\gamma_1, \ldots, \gamma_n]^\top \in \mathbb{T}^n$, with dc voltage vector $v_{\rm dc} = [v_{{\rm dc},1}, \ldots, v_{{\rm dc},n}]^\top \in \mathbb{R}^n$, the inductance current $i = [i_1^\top, \ldots, i_n^\top]^\top \in \mathbb{R}^{2n}$ and ac capacitor voltage $v = [v_1^\top, \ldots, v_n^\top]^\top \in \mathbb{R}^{2n}$. The last equation in (3) describes the line dynamics and in particular, the evolution of the line current $i_\ell := [i_{\ell_1}^\top, \ldots, i_{\ell_m}^\top]^\top \in \mathbb{R}^{2m}$, where $R_\ell > 0$ is the line resistance, $L_\ell > 0$ is the line inductance and $i_{\rm net} = \mathbf{B}\, i_\ell$. Here, $\mathbf{B} = \mathcal{B} \otimes I$ denotes the extended incidence matrix and $K = {\rm diag}(\mathbf{I}, C_{\rm dc}\,\mathbf{I}, L\,\mathbf{I}, C\,\mathbf{I}, L_\ell\,\mathbf{I})$. The multiconverter inputs are collected in $\mathbf{u} = [i^*_{{\rm dc},1}, \ldots, i^*_{{\rm dc},n}]^\top \in \mathbb{R}^n$.

Let N be the dimension of the state vector $z = [\gamma^\top\ \tilde v_{\rm dc}^\top\ x_{\rm ac}^\top]^\top$, whereby we define the vectors of relative dc voltage $\tilde v_{\rm dc} = v_{\rm dc} - v^*_{\rm dc}\mathbb{1}_n$, ac quantities $x_{\rm ac} = [i^\top\ v^\top\ i_\ell^\top]^\top$ and the input $u = [0^\top, \mathbf{u}^\top, \ldots, 0^\top]^\top$. By putting it all together, we arrive at the nonlinear power system dynamics compactly described by

$$\dot z = f(z, u)\,, \quad z(0) = z_0\,. \tag{4}$$

Here, $z, z_0 \in \mathbb{R}^N$, and $f(z, u)$ denote the vector field given by (3).

Remark 1: Without loss of generality, we assume that all dc/ac converters are identical and connected via identical *RL* lines, that is a common assumption in the analysis of power system stability, see, e.g., [9], [15]. Nonetheless, our analysis carries over to more general heterogeneous settings, where converters and lines differ in their parameter values.

III. Characterization of the Steady-State Set

In this section, we characterize the steady-state set resulting from the rotational invariance of the vector field (4) and feasible dc inputs to the converters as a mapping from known steady state angles.

A. Steady-State Set

Let $\mathcal{M} \subset \mathbb{R}^N$ be a nonempty steady-state manifold resulting from setting (4) to zero and given by

$$\mathcal{M} = \{z^* \in \mathbb{R}^N \mid f(z^*, u) = 0\}. \tag{5}$$

We are particularly interested in a synchronous steady state in rotating $dq-$frame with the following properties:

1) The converters' frequencies are synchronized at the nominal value ω^* mapped into a nominal dc voltage $v_{\rm dc}^* \geq 1$

$$[\omega] = \{\omega \in \mathbb{R}^n_{\geq 0} |\, \omega = \omega^* \mathbb{1}_n\}$$

$$[v_{\rm dc}] = \{v_{\rm dc} \in \mathbb{R}^n_{\geq 0} |\, v_{\rm dc} = v_{\rm dc}^* \mathbb{1}_n\}\,.$$

2) The converters' angles are stationary

$$[\gamma] = \{\gamma \in \mathbb{T}^n |\, \dot{\gamma}^* = 0\}\,.$$

3) The ac quantities, namely the inductor currents, capacitor voltages, and line currents are constant at steady state

$$[x_{\rm ac}] = \left\{x_{\rm ac} \in \mathbb{R}^{4n+2m} |\, \dot{x}_{\rm ac}^* = 0\right\}\,.$$

B. Symmetry of the Vector Field

Consider the nonlinear power system model (4). For all $\theta \in \mathbb{S}^1$, it holds that

$$f(\theta\, s_0 + S(\theta)\, z, u) = S(\theta)\, f(z, u) \tag{6}$$

where we define the translation vector $s_0 = \left[\, \mathbb{1}_n^\top \; 0^\top \; 0^\top \,\right]^\top$, the matrix $S(\theta) = \begin{bmatrix} \mathbf{I} & 0 & 0 \\ 0 & \mathbf{I} & 0 \\ 0 & 0 & \mathbf{R}(\theta) \end{bmatrix}$, and the set

$$\mathcal{S}(z) = \left\{ \left[\, (\gamma + \theta \mathbb{1}_n)^\top \; \tilde{v}_{\rm dc}^\top \; (\mathbf{R}(\theta)\, x)^\top \,\right]^\top,\, \theta \in \mathbb{S}^1 \right\}. \tag{7}$$

The symmetry (6) follows from observing that the rotation matrix $\mathbf{R}(\theta)$ commutes with the impedance and admittance matrices Z_R, Z_ℓ, Y_C, the skew-symmetric matrix $\mathbf{J}$ and the incidence matrix $\mathbf{B}$. The symmetry (6) arises from knowing that the nonlinear power system model (4) has no absolute angle. In fact, the vector field remains invariant with respect to a shift in all angles $\gamma \in \mathbb{T}^n$, corresponding to a translation by s_0 and a rotation in the angles of ac signals by $\mathbf{R}(\theta)$ (up to redefining the $dq-$transformation angle to $\theta'_{dq}(t) = \theta_{dq}(t) + \theta$). Notice that for $\theta = 0$, we deduce that $\mathcal{S}(z) = \{z\}$ and hence $z \in \mathcal{S}(z)$.

Consider the steady-state manifold $\mathcal{M}$ described by (5). Observe that $z^* \in \mathcal{M}$ pertains to a continuum of steady states, as a consequence of the rotational symmetry (6). Thus, the steady-state set is given by

$$\mathcal{S}(z^*) = \left\{ \left[\, (\gamma^* + \theta \mathbb{1}_n)^\top \, 0^\top \, (\mathbf{R}(\theta)\, x_{\rm ac}^*)^\top \,\right]^\top,\, \theta \in \mathbb{S}^1 \right\} \tag{8}$$

that is for all $z^* \in \mathcal{M}$, it holds that $\mathcal{S}(z^*) \subset \mathcal{M}$.

C. Steady-State Map

Lemma III.1 (Steady-State Map): Consider the nonlinear power system model (4). Given the steady-state angle vector γ^* satisfying $\dot{\gamma}^* = 0$. Then, a feasible input $\mathbf{u}$ is given by

$$\mathbf{u} = \nu\, \mathrm{Rot}(\gamma^*)^\top \mathcal{Y}\, \mathrm{Rot}(\gamma^*)\, \mathbb{1}_n \tag{9}$$

where $\nu = \frac{1}{4}\mu^2 v_{dc}^* > 0$ and $\mathcal{Y} = (Z_R + (Y_C + \mathbf{B}\, Z_\ell^{-1}\, \mathbf{B}^\top)^{-1})^{-1} \in \mathbb{R}^{2n \times 2n}$.

Proof: We solve for the frequency synchronous steady state z^* by setting (4) to zero. Note that $Y_C + \mathbf{B}\, Z_\ell^{-1} \mathbf{B}^\top$ and $Z_R + (Y_C + \mathbf{B}\, Z_\ell^{-1}\, \mathbf{B}^\top)^{-1}$ are nonsingular matrices due to the presence of the load conductance $G > 0$ and the resistance $R > 0$, where $\mathbf{B}\, Z_\ell^{-1} \mathbf{B}^\top$ is a weighted Laplacian matrix. The lines' current vector is described by $i_\ell^* = Z_\ell^{-1}\, \mathbf{B}^\top v^*$, from which follows that $v^* = (Y_C + \mathbf{B} Z_\ell^{-1}\, \mathbf{B}^\top)^{-1} i^*$ for the ac capacitor voltage. The inductance current reads as $i^* = \frac{1}{2} v_{\rm dc}^*\, \mu\, \mathcal{Y}\, \mathrm{Rot}(\gamma^*)\, \mathbb{1}_n$. Finally, from $\frac{1}{2}\mu \mathrm{Rot}^\top(\gamma^*) i^* = \mathbf{u}$, we deduce (9). ■

Notice that the matrix $\mathcal{Y}$ in (9) has an *admittance-like* structure, which is customary in the analysis of power system models and encodes in particular the parameters of the transmission lines and the network topology given by the weighted Laplacian $\mathbf{B}\, Z_\ell^{-1}\, \mathbf{B}^\top$, as well as the converters' parameters (their ac filters, namely given by the impedance and admittance matrices Z_R and Y_C). Once $\gamma^* \in \mathbb{T}^n$ is given, we recover the full vector $z^* \in \mathcal{M}$ associated with a frequency synchronous steady-state set $\mathcal{S}(z^*)$ as described in (8).

Equation (9) can be comprehended as a map (in the sense of [16])

$$\mathcal{P} : \mathbb{T}^n \to \mathbb{R}^n,\; \gamma^* \mapsto \nu\, \mathrm{Rot}(\gamma^*)^\top \mathcal{Y}\, \mathrm{Rot}(\gamma^*)\, \mathbb{1}_n$$

that takes as argument γ^* and returns a feasible input $\mathbf{u}$. The angles γ^* can be obtained, e.g., from solving an ac optimal power flow problem. Equation (9) indicates a power balance between the electrical power $P_e^* = \nu\, v_{\rm dc}^*\, \mathrm{Rot}^\top(\gamma^*)\, i^*$ and the dc power given by $P_{\rm dc}^* = v_{\rm dc}^* \mathbf{u}$ at steady state.

IV. Local Synchronization of Multiconverter Power System

In this section, we study local asymptotic stability of the steady-state set $\mathcal{S}(z^*)$ in (8), as an application of center manifold theory [13], [17, p. 195].

A. Preliminaries

We provide some background and review key concepts from center manifold theory [17] that serve as our main tool for proving local asymptotic stability. For this, consider a dynamical system given in normal form

$$\dot{y} = A_y y + f_1(y, \rho) \tag{10a}$$

$$\dot{\rho} = B_\rho \rho + f_2(y, \rho) \tag{10b}$$

where $A_y \in \mathbb{R}^{c \times c}$ has eigenvalues with zero real part and $B_\rho \in \mathbb{R}^{(n-c)\times(n-c)}$ has eigenvalues with negative real part (or Hurwitz), and f_1 and f_2 are nonlinear functions with the following properties:

$$f_1(0,0) = 0, \quad J_{f_1}(0,0) = 0 \tag{11}$$

$$f_2(0,0) = 0, \quad J_{f_2}(0,0) = 0. \tag{12}$$

An invariant manifold $\mathcal{W}^c$ is a center manifold of (10), if it can be locally expressed as

$$\mathcal{W}^c = \{(y, \rho) \in \mathcal{W}^0 |\, \rho = h(y)\} \tag{13}$$

where $\mathcal{W}^0$ is a sufficiently small neighborhood of the origin, $h(0) = 0$ and

$$J_h(0) = \frac{\mathrm{d}\, h}{\mathrm{d}\, y}\bigg|_{y=0} = 0\,.$$

It has been shown in [10, Th. 8.1] that a center manifold always exists and the dynamics of (10) restricted to the center manifold are described by

$$\dot{\xi} = A_y\,\xi + f_1(\xi, h(\xi)) \tag{14}$$

for a sufficiently small $\xi \in \mathbb{R}^c$. Note that ξ is a parametric representation of the dynamics along points on the center manifold $\mathcal{W}^c$ in (13).

The stability of the system dynamics (10) is analyzed from the dynamics on the center manifold (13) using the reduction principle described in the following theorem.

Theorem IV.1 (see [13], p.195): If the origin is stable under (14), then the origin of (10) is also stable. Moreover there exists a neighborhood $\mathcal{W}^0$ of the origin, such that for every $(y(0), \rho(0)) \in \mathcal{W}^0$, there exists a solution $\xi(t)$ of (14) and constants $c_1, c_2 > 0$ and $\gamma_1, \gamma_2 > 0$ such that

$$y(t) = \xi(t) + r_1(t)$$
$$\rho(t) = h(\xi(t)) + r_2(t)$$

where $\|r_i(t)\| < c_i\, e^{-\gamma_i t}$, $i = 1, 2$.

Next, we provide background on set stability in the following definition.

Definition IV.2 (Set Stability [18]): A set $\mathcal{K}$ is called stable with respect to the dynamical system (4), if for all $\epsilon > 0$, there exists $\delta > 0$, so that

$$d(z_0, \mathcal{K}) \leq \delta \Rightarrow d(z(t, z_0), \mathcal{K}) < \epsilon, \quad \forall t \geq 0. \tag{15}$$

A set $\mathcal{K}$ is called *asymptotically stable* with respect to a dynamical system (4), if (15) holds and

$$\lim_{t\to\infty} d(z(t, z_0), \mathcal{K}) = 0.$$

B. Local Asymptotic Stability

Next, we present our main result concerning local asymptotic stability of the set $\mathcal{S}(z^*)$ with respect to the power system dynamics (4). The following assumption on the eigenvalues of the Jacobian of (4) is crucial for our result.

Assumption 1: Consider the multi-converter system (4) linearized at $z^* \in \mathcal{M}$ and given by

$$\delta\dot{z} = J_f(z^*)\,\delta z \tag{16}$$

with $\delta z = z - z^* \in T_{z^*}\mathcal{M}$, $J_f(z^*) = \frac{\mathrm{d}f}{\mathrm{d}z}\,|_{z=z^*}$ its Jacobian matrix. Assume that $J_f(z^*)$ has only one eigenvalue at zero and all other eigenvalues are in the open-left half-plane.

Remark 2: In Section V, we suggest one possible approach to satisfy the Jacobian eigenvalues' condition in Assumption 1 that leads to sufficient and explicit stability conditions.

We now present our main result in the following theorem.

Theorem IV.3 (Local Asymptotic Stability): Consider the power system dynamics in (4) under Assumption 1 with a feasible input $\mathbf{u}$ as in (9). Then, $\mathcal{S}(z^*)$ is locally asymptotically stable. Moreover, there exists a neighborhood $\mathcal{N}$ of $\mathcal{S}(z^*)$ such that for every $z(0) \in \mathcal{N}$, there exists a point $s \in \mathcal{S}(z^*)$, where

$$\lim_{t\to\infty} z(t, z_0) = s.$$

Proof: To prove that $\mathcal{S}(z^*)$ is stable, we consider the system dynamics (4) under Assumption 1. Without loss of generality, assume $z^* = 0$. From Assumption 1, we know there exists a transformation $T \in \mathbb{R}^{N\times N}$, such that $T\,J_f(0)\,T^{-1}$ is block diagonal, where $J_f(0)$ is given in (16), with zero for the first vector component and a block diagonal matrix B that is Hurwitz. We rewrite the dynamics of (4) as

$$\dot{z} = J_f(0)\,z + (f(z, u) - J_f(0)\,z)$$

where z is near the origin. Next, by defining $(y, \rho) = T\,z$, we arrive at the following system dynamics in normal form:

$$\dot{y} = f_1(y, \rho) \tag{17a}$$
$$\dot{\rho} = B\,\rho + f_2(y, \rho) \tag{17b}$$

where $f_1(0, 0) = 0$, $f_2(0, 0) = 0$, and $J_{f_1}(0, 0) = J_{f_2}(0, 0) = 0$. Now, we show that

$$\mathcal{W}^c := \{(y, \rho) | (\exists\, z \in \mathcal{S}(0)) \times ((y, \rho) = T\,z)\}$$

is a center manifold for the system dynamics (17). First, $\mathcal{W}^c$ is invariant because it consists of steady states of (17). Second, $\mathcal{W}^c$ is tangent to the $y-$axis at $y = 0$. To see this, define

$$\tilde{f}(y, \rho) := f\left(T^{-1}\begin{bmatrix} y \\ \rho \end{bmatrix}\right) = f(z).$$

Then, $\mathcal{W}^c = \{(y, \rho) | \tilde{f}(y, \rho) = 0\}$. The row vectors of the Jacobian given by

$$J_{\tilde{f}}(0, 0) = \begin{bmatrix} \frac{\partial \tilde{f}_1(0,0)}{\partial y} & \frac{\partial \tilde{f}_1(0,0)}{\partial \rho} \\ \vdots & \vdots \\ \frac{\partial \tilde{f}_N(0,0)}{\partial y} & \frac{\partial \tilde{f}_N(0,0)}{\partial \rho} \end{bmatrix} = \frac{\mathrm{d}f}{\mathrm{d}z}\Big|_{z=0} T^{-1} = J_f(0)\,T^{-1}$$

span the normal space of $\mathcal{W}^c$ at 0. Since the columns of $T^{-1} = (v(0), \dots)$ consist of the right eigenvectors of $J_f(0)$, by means of $J_f(0)\,v(0) = 0$, $J_f(0)\,T^{-1}$ has a zero first column. This shows that $J_{\tilde{f}}(0, 0)$ has its first entry (corresponding to $y-$component) equal to zero. As a consequence, there exists a function $h(y)$ such that $h(0) = 0$ and $\frac{\mathrm{d}h}{\mathrm{d}y}|_{y=0} = 0$ in a neighborhood $\mathcal{W}^0$ of 0, where $\mathcal{W}^c \cap \mathcal{W}^0 = \{(y, \rho) |\, \rho = h(y)\}$. It follows that the dynamics restricted to $\mathcal{W}^0$ are given by $\dot{\xi} = 0$ because $\mathcal{W}^c$ is a steady-state manifold to (17) and thus $f_1(\xi, h(\xi)) = 0$. This shows that $\xi(t) = \xi(0)$. By applying Theorem IV.1, the solutions for (y, ρ) starting in $\mathcal{W}^0$ are described by

$$y(t) = \xi(t) + r_1(t)$$
$$\rho(t) = h(\xi(t)) + r_2(t)$$

where $\|r_i(t)\| < c_i e^{-\gamma_i t}$, $i = 1, 2$, for some constants $c_i, \gamma_i > 0$. This implies that

$$\lim_{t\to\infty} (y(t), \rho(t)) = (\xi(0), h(\xi(0)))$$

and thus

$$\lim_{t\to\infty} z(t) = T^{-1}\,(\xi(0), h(\xi(0))) \in \mathcal{S}(0).$$

This argument can be repeated for each point on $\mathcal{S}(0)$ to obtain a cover $\{\mathcal{W}^k\}$ of $\mathcal{S}(0)$. Since $\mathcal{S}(0)$ is compact, we can construct

a finite subcover to form a neighborhood $\mathcal{N} = \bigcup_k \mathcal{W}^k$ of $\mathcal{S}(0)$. Local asymptotic stability of $\mathcal{S}(0)$ follows directly. ■

Note that our results conceptually apply to prove local asymptotic stability of a synchronous steady-state set with respect to trajectories of high-order dynamics of synchronous machines and find an estimate of their region of attraction. Even though our analysis dwells upon a local statement, it can pave the way for a global analysis of the stability of high-order multi-machine or multi-converter system connected through nontrivial lines' conductance, which has been an open problem within the power system community for a long time [19], [20].

V. Sufficient Conditions for Stability of the Linearized System

This section suggests one possible approach to satisfy the eigenvalue condition imposed by Assumption 1 in a sufficient and explicit way for a class of linear systems, that applies later to the stability of the linearized multi-converter system.

A. Lyapunov Stability of Vector Fields With Symmetries

We develop a stability theory for a general class of linear systems enjoying some of the structural properties featured by the Jacobian matrix (16). For this, we consider a class of partitioned linear systems of the form

$$\dot{x} = \underbrace{\left[\begin{array}{c|c} A_{11} & A_{12} \\ \hline A_{21} & A_{22} \end{array}\right]}_{A} x \tag{18}$$

where $x = [x_1^\top \; x_2^\top]^\top$ denotes the partitioned state vector and the block matrices $A_{11}, A_{12}, A_{21}, A_{22}$ are of appropriate dimensions.

In the following, we assume stability of the subsystem characterized by A_{11} and the existence of a symmetry, i.e., an invariant zero eigenspace of A.

Assumption 2: The block diagonal matrix A_{11} given in (18) is Hurwitz.

Assumption 3: There exists a vector $p = [p_1^\top \; p_2^\top]^\top$, so that

$$A \cdot \text{span}\{p\} = 0.$$

We are interested in asymptotic stability of the zero subspace span$\{p\}$. This is equivalent to showing that, all eigenvalues of A have their real part in the open-left half-plane except for only one at zero, whose eigenspace is span$\{p\}$. In this manner, we later satisfy Assumption 1. Recall that the standard stability definitions and Lyapunov methods extend from stability of the origin to stability of closed and invariant sets when using the point-to-set-distance rather than merely the norm in the comparison functions; see e.g., [21, Th. 2.8]. In our case, we seek a quadratic Lyapunov function that vanishes on span$\{p\}$, is positive elsewhere and whose derivative is decreasing everywhere outside span$\{v\}$. We start by defining a Lyapunov function candidate

$$V(x) = x^\top \left(P - \frac{Ppp^\top P}{p^\top P p}\right) x \tag{19}$$

where P is *a positive definite* matrix. The Lyapunov function candidate constructed in (19) is based on *two* key observations:

1) First, the function $V(x)$ is defined via an oblique projection of the vector $x \in \mathbb{R}^n$ parallel to span$\{p\}$ onto $\{x \in \mathbb{R}^n | \, p^\top P x = 0\}$. If $P = \mathbf{I}$, then V is the *orthogonal projection onto* span$\{p\}^\perp$. Hence, $V(x)$ vanishes on span$\{p\}$ and is strictly positive definite elsewhere.
2) Second, the positive definite matrix P is *a degree of freedom* that can be specified later to provide sufficient and explicit stability conditions.

In standard Lyapunov analysis, one seeks a pair of matrices $(P, \mathcal{Q})$ with suitable positive (semi-) definiteness properties so that the Lyapunov equation $PA + A^\top P = -\mathcal{Q}$ is met. In the following, we apply a helpful twist and parameterize the $\mathcal{Q}$ matrix as a quadratic function $\mathcal{Q}(P)$ of P, which renders the Lyapunov equation, in part, an $\mathcal{H}_\infty-$ARE. We choose the following structure for the matrix $\mathcal{Q}(P)$

$$\mathcal{Q}(P) = \begin{bmatrix} \mathcal{Q}_1 & H^\top(P) \\ H(P) & H(P)\mathcal{Q}_1^{-1}H(P)^\top + \mathcal{Q}_2 \end{bmatrix} \tag{20}$$

where $\mathcal{Q}_1$ is a positive definite matrix, $\mathcal{Q}_2$ is a positive semidefinite matrix with respect to span$\{p_2\}$, P is block-diagonal

$$P = \begin{bmatrix} P_1 & 0 \\ 0 & P_2 \end{bmatrix} \tag{21}$$

with $P_1 = P_1^\top > 0$ and $P_2 = P_2^\top > 0$, i.e., the Lyapunov function is *separable*, and finally $H(P) = A_{12}^\top P_1 + P_2 A_{21}$ is a shorthand.

We need to introduce a third and final assumption.

Assumption 4: Consider the matrix $F = A_{22} + A_{21}\mathcal{Q}_1^{-1}P_1A_{12}$ and the transfer function

$$\mathcal{G} = \mathcal{C}\,(s\,\mathbf{I} - F)^{-1}\,B$$

with $B = A_{21}\mathcal{Q}_1^{-1/2}$, $\mathcal{C} = (A_{12}^\top P_1 \mathcal{Q}_1^{-1} P_1 A_{12} + \mathcal{Q}_2)^{1/2}$. Assume that F is Hurwitz and $\|\mathcal{G}\|_\infty < 1$.

Assumption 4 will guarantee suitable definiteness and decay properties of the Lyapunov function (21) under sufficient and explicit stability conditions discussed in Section V-C. Assumptions 2–4 recover our requirement for positive definiteness of the matrix P in (21) and semidefinitness (with respect to span$\{p\}$) of $\mathcal{Q}(P)$ in (20) as shown in the following.

Corollary V.1: Under Assumptions 2–4, the matrix P in (21) exists, is unique and positive definite.

Proof.: By calculating $PA + A^\top P = -\mathcal{Q}(P)$, where A, $\mathcal{Q}(P)$, and P are given, respectively, by (18), (20), and (21), we obtain

$$\begin{bmatrix} P_1 A_{11} + A_{11}^\top P_1 & H(P)^\top \\ H(P) & P_2 A_{22} + A_{22}^\top P_2 \end{bmatrix} = -\begin{bmatrix} \mathcal{Q}_1 & H(P)^\top \\ H(P) & H(P)\mathcal{Q}_1^{-1}H(P)^\top + \mathcal{Q}_2 \end{bmatrix}$$

the block-diagonal terms of which are

① $P_1 A_{11} + A_{11}^\top P_1 = -\mathcal{Q}_1$
② $P_2 A_{22} + A_{22}^\top P_2 = -H(P)\mathcal{Q}_1^{-1}H(P)^\top - \mathcal{Q}_2$

where $H(P) = A_{12}^\top P_1 + P_2 A_{21}$. Since A_{11} is Hurwitz, there is a unique and positive definite matrix P_1 solving ①.

Moreover, ② is equivalent to solving for P_2 the following $\mathcal{H}_\infty-$ARE

$$P_2 A_{21}\mathcal{Q}_1^{-1}A_{21}^\top P_2 + P_2 F + F^\top P_2 + A_{12}^\top P_1 \mathcal{Q}_1^{-1} P_1 A_{12} + \mathcal{Q}_2 = 0$$

where $F = A_{22} + A_{21}\mathcal{Q}_1^{-1}P_1 A_{12}$. Under Assumption 4, the pair (F, B) is stabilizable with $B = A_{21}\mathcal{Q}_1^{-1/2}$ and for $\|\mathcal{G}\|_\infty < 1$, [22, Th. 7.4] implies that no eigenvalues of the Hamiltonian matrix $\mathcal{H} = \begin{bmatrix} F & B\,B^\top \\ -\mathcal{C}^\top\mathcal{C} & -F^\top \end{bmatrix}$ are on the imaginary axis with $\mathcal{C} = (A_{12}^\top P_1 \mathcal{Q}_1^{-1} P_1 A_{12} + \mathcal{Q}_2)^{1/2}$. By [22, Th. 7.2], there exists a unique stabilizing solution P_2 to ② Define $E = A_{12}^\top P_1 \mathcal{Q}_1^{-1} P_1 A_{12} + \mathcal{Q}_2 + P_2\, A_{21}\mathcal{Q}_1^{-1}A_{21}^\top P_2 \geq 0$. From $Ap = 0$, follows that $A_{12}p_2 = -A_{11}p_1 \neq 0$ (by Hurwitzness of A_{11} under Assumption 2) and since $\mathcal{Q}_2 p_2 = 0$, this implies that $\ker \mathcal{Q}_2 \cap \ker A_{12} = \{0\}$. Therefore, E is a nonsingular and positive definite matrix. Since F is Hurwitz, by standard Lyapunov theory [10], the Lyapunov equation $P_2\, F + F^\top P_2 + E = 0$ admits a positive definite solution P_2. ■

Corollary V.2: Under Assumptions 2–4, the matrix $\mathcal{Q}(P)$ in (20) is positive semidefinite. Additionally, $\ker(A) = \ker(\mathcal{Q}(P)) = \text{span}\{p\}$.

Proof.: First, note that by Proposition V.1, the matrix $P = P^\top > 0$ and observe that the matrix $\mathcal{Q}(P)$ in (20) is symmetric and the upper left block $\mathcal{Q}_1 > 0$ is positive definite. By using the Schur complement and positive semidefiniteness of $\mathcal{Q}_2$, we obtain that $\mathcal{Q}(P)$ is positive semidefinite. Second, by virtue of $p^\top \mathcal{Q}(P) p = p^\top (P\,A + A^\top P)p = 0$ due to Assumption 3, it follows that $\text{span}\{p\} \subseteq \ker(\mathcal{Q}(P))$. Third, consider a general vector $s = [s_1^\top \;\; s_2^\top]^\top$, so that $\mathcal{Q}(P)s = 0$. Given $H(P) = A_{12}^\top P_1 + P_2\, A_{21}$, we obtain the algebraic equations $\mathcal{Q}_1 s_1 + H(P)^\top s_2 = 0$, $H(P)s_1 + (H(P)\mathcal{Q}_1^{-1}H(P)^\top + \mathcal{Q}_2)s_2 = 0$. One deduces that $\mathcal{Q}_2 s_2 = 0$ and thus $s_2 \in \text{span}\{p_2\}$. The latter implies $s_1 \in -\mathcal{Q}_1^{-1}H(P)^\top \text{span}\{p_2\} \in \text{span}\{p_1\}$ because $\mathcal{Q}(P)\text{span}\{p\} = 0$. Thus, it follows that $s \in \text{span}\{[s_1^\top \;\; s_2^\top]^\top\} = \text{span}\{p\}$ and we deduce that $\ker(\mathcal{Q}(P)) = \text{span}\{p\}$. Fourth and finally, for the sake of contradiction, take a vector $\tilde{v} \notin \text{span}\{p\}$, so that $\tilde{v} \in \ker(A) \Rightarrow \tilde{v}^\top(A^\top P + P\,A)\tilde{v} = 0 \Rightarrow \tilde{v}^\top \mathcal{Q}(P)\tilde{v} = 0 \Rightarrow \tilde{v} \in \ker(\mathcal{Q}(P))$. This is a contradiction to $\ker(\mathcal{Q}(P)) = \text{span}\{p\}$. Hence, we conclude that $\ker(A) = \ker(\mathcal{Q}(P)) = \text{span}\{p\}$. ■

The main result of this section is given by the following lemma.

Lemma V.3: Consider the linear system (18). Under Assumptions 2–4, $\text{span}\{p\}$ is an asymptotically stable subspace of A.

Proof: Consider the function $V(x)$ in (19). The matrix P in (21) is positive definite by Proposition V.1. By taking $y = P^{1/2}x$ and $w = P^{1/2}p$, the function $V(x)$ can be rewritten as

$$V(y) = y^\top(\mathbf{I} - \frac{ww^\top}{w^\top w})y = y^\top \Pi_w y.$$

The matrix

$$\Pi_w = \mathbf{I} - \frac{ww^\top}{w^\top w}$$

is a projection matrix onto the orthogonal complement of $\text{span}(w)$ and is hence positive semidefinite with 1-D nullspace corresponding to $P^{1/2}\text{span}\{p\}$. It follows that the function $V(x)$ is positive definite for all $x \in \text{span}\{p\}^\perp$. By means of $Ap = \mathcal{Q}(P)p = 0$, it holds that $p^\top P\, A = p^\top(\mathcal{Q}(P) - A^\top P) = 0$ and we obtain $\dot{V}(x) = -x^\top\, \mathcal{Q}(P)\, x$. By Lemma V.2, $\dot{V}(x)$ is negative definite for all $x \in \text{span}\{p\}^\perp$. We apply Lyapunov's method and [21, Th. 2.8] to conclude that $\text{span}\{p\}$ is asymptotically stable. ■

B. Stability of the Linearized Multi-DC/AC Converter

Our next analysis seeks to find sufficient and explicit conditions, so that the Jacobian of the multi-converter system given in (16) satisfies Assumption 1. For this, consider the linearized system (16) given by the following equations:

$$\delta\dot{z} = K^{-1}\left[\begin{array}{cc|ccc} 0 & \eta\mathbf{I} & 0 & 0 & 0 \\ -\nabla^2 U(\gamma^*) & -K_p\mathbf{I} & -\Lambda(\gamma^*)^\top & 0 & 0 \\ \hline \Xi(\gamma^*) & \Lambda(\gamma^*) & -Z_R & -\mathbf{I} & 0 \\ 0 & 0 & \mathbf{I} & -Y_C & -\mathbf{B} \\ 0 & 0 & 0 & \mathbf{B}^\top & -Z_\ell \end{array}\right]$$

$$\delta z = \left[\begin{array}{c|c} A_{11} & A_{12} \\ \hline A_{21} & A_{22} \end{array}\right]\delta z. \tag{22}$$

In (22), the system matrix is the Jacobian $J_f(z^*) = \frac{\mathrm{d}f}{\mathrm{d}z}\,|_{z=z^*}$, $\delta z = [\,\delta z_1^\top \;\delta z_2^\top\,]^\top \in T_{z^*}\mathcal{M}$, corresponding to the partition $\delta z_1 = [\,\delta\gamma^\top \;\delta v_{dc}^\top\,]^\top \in \mathbb{R}^{2n}$, $\delta z_2 \in \mathbb{R}^{6n}$. Moreover, the matrices are given by

$$\begin{aligned} \nabla^2 U(\gamma^*) &= \frac{1}{4}\mu^2 v_{dc}^* \text{diag}(\text{Rot}^\top(\gamma^*)\,\mathbf{J}^\top \mathcal{Y}\,\text{Rot}(\gamma^*)\,\mathbb{1}_n) \\ &= \frac{1}{2}\mu \text{diag}((\mathbf{J}\text{Rot}(\gamma^*))^\top i^*) \\ \Xi(\gamma^*) &= \frac{1}{2}\mu \mathbf{J}\,\text{Rot}(\gamma^*) \\ \Lambda(\gamma^*) &= \frac{1}{2}\mu v_{dc}^*\,\text{Rot}(\gamma^*) \end{aligned}$$

where we consider the smooth potential function

$$U : \mathbb{T}^n \to \mathbb{R},\ \gamma \mapsto -\xi\,\mathbb{1}_n^\top\,\text{Rot}^\top(\gamma)\,\mathbf{J}^\top \mathcal{Y}\,\text{Rot}(\gamma^*)\,\mathbb{1}_n.$$

Note that the Jacobian $J_f(z^*)$ has 1-D zero eigenspace denoted by

$$\text{span}\{v(z^*)\} = \text{span}\left\{\left[\,\mathbb{1}_n{}^\top\; 0^\top\; (\mathbf{J}\,x^*)^\top\,\right]^\top\right\} \subset T_{z^*}\mathcal{M}$$

with $\mathbf{J}\,x^* = [\,(\mathbf{J}\,i^*)^\top\;(\mathbf{J}v^*)^\top\;(\mathbf{J}\,i_\ell^*)^\top\,]^\top$. In fact, we can establish a formal link between the linear subspace $\text{span}\{v(z^*)\}$ and the steady-state set $\mathcal{S}(z^*)$ in (8) as follows. For all $\theta \in \mathbb{S}^1$

$$\mathcal{S}(z^*) = z^* + \int_0^\theta v(z^*)\,\mathrm{d}s = z^* + \int_0^\theta \begin{bmatrix} \mathbb{1}_n \\ 0 \\ \mathbf{J}\,\mathbf{R}(s)\,x^* \end{bmatrix}\mathrm{d}s\,.$$

In fact, $v(z^*)$ is the tangent vector of $\mathcal{S}(z^*)$ in the $\theta-$direction and lies on the tangent space $T_{z^*}\mathcal{M}$ and $\mathcal{S}(z^*)$ is the angle integral curve of $\text{span}\{v(z^*)\}$.

Remark 3: We can retrieve the relationship $\text{span}\{v(z^*)\} \subseteq \ker(J_f(z^*))$ from (6) as follows. We set $z = z^* \in \mathcal{M}$ and expand the first-order Taylor polynomial around $\theta' \in \mathbb{S}^1$ of the

left-hand side in (6). The right-hand side amounts to zero since $f(z^*, u) = 0$ and we obtain

$$\left.\frac{\mathrm{d}f}{\mathrm{d}z}\right|_{z=z^*} \left(s_0 + \left.\frac{\mathrm{d}S(\theta)}{\mathrm{d}\theta}\right|_{\theta=\theta'} z^* \right) (\theta - \theta') = 0$$

where $\frac{\mathrm{d}f}{\mathrm{d}z}\,|_{z=z^*} = J_f(z^*)$, $s_0 + \frac{\mathrm{d}S}{\mathrm{d}\theta}|_{\theta=\theta'} z^* = v(z^*)$. Thus, we recover

$$J_f(z^*)\, v(z^*) = 0\,.$$

Next, we consider the linearized model (22) and identify the matrices

$$A_{11} = \begin{bmatrix} 0 & \eta\mathbf{I} \\ -C_{\mathrm{dc}}^{-1}\nabla^2 U(\gamma^*) & -C_{\mathrm{dc}}^{-1}K_p\mathbf{I} \end{bmatrix}$$

$$A_{12} = \begin{bmatrix} 0 & 0\,0 \\ -C_{\mathrm{dc}}^{-1}\Lambda(\gamma^*)^\top & 0\,0 \end{bmatrix}$$

$$A_{21} = \begin{bmatrix} L^{-1}\Xi(\gamma^*) & L^{-1}\Lambda(\gamma^*) \\ 0 & 0 \\ 0 & 0 \end{bmatrix}$$

$$A_{22} = \begin{bmatrix} -L^{-1}\mathbf{Z}_R & -L^{-1}\mathbf{I} & 0 \\ C^{-1}\mathbf{I} & -C^{-1}\mathbf{Z}_V & -C^{-1}\mathbf{B} \\ 0 & L_\ell^{-1}\mathbf{B}^\top & -L_\ell^{-1}\mathbf{Z}_\ell \end{bmatrix}.$$

Define the Lyapunov function $V(z)$ as in (19) with $v(z^*) := p$ and $v(z^*) = [v_1^{*\top}, v_2^{*\top}]^\top$. Hence, $V(z)$ is positive semidefinite with respect to span$\{v(z^*)\}$. Next, we select the matrix $\mathcal{Q}(P)$ given by (20), set $\mathcal{Q}_1 = \mathbf{I}$, $\mathcal{Q}_2 = \mathbf{I} - v_2^* v_2^{*\top}/v_2^{*\top}v_2^*$ and search for the positive definite matrix P so that

$$P\, J_f(z^*) + J_f(z^*)^\top P = -\mathcal{Q}(P).$$

Similar to (21), we choose the block diagonal matrix as

$$P = \left[\begin{array}{cc|c} P_{11} & P_{12} & 0 \\ P_{12} & P_{22} & 0 \\ \hline 0 & 0 & P_{33} \end{array}\right] = \left[\begin{array}{c|c} P_1 & 0 \\ \hline 0 & P_2 \end{array}\right]. \tag{23}$$

Here, P_{11}, P_{12}, and P_{22} are matrices of appropriate dimensions. Notice that the chosen structure of P_1 and the zeros in the off-diagonals in P originate from the physical intuition of the tight coupling between the angle of the converter and its corresponding dc voltage (proportional to the ac frequency), as enabled by the matching control (1). The same type of coupling comes into play in synchronous machines between the rotor angle and its frequency, due to the presence of the electrical power in the swing equation [2]. The matrix P_2 is dense with off-diagonals coupling at each phase, the inductance current of one converter with the others. In the sequel, we show that this structure allows to derive sufficient and explicit conditions that satisfy Assumption 1.

Condition V.4 (Parametric Synchronization Conditions): Consider $P_{x,k} = \frac{1}{2}v_{\mathrm{dc}}^*\mu r^\top(\gamma_k^*)i_k^* > 0$, $Q_{x,k} = \frac{1}{2}v_{\mathrm{dc}}^*\mu r^\top(\gamma_k^*)J^\top i_k^* > 0$ and the matrix F in Assumption 4. Assume the following condition is satisfied:

$$\cos(\phi_k) < \sqrt{1 - \frac{\alpha^2}{P_{x,k}^2 + \alpha^2}}, \quad k = 1, \ldots, n \tag{24}$$

where $\cos(\phi_k) = \frac{P_{x,k}}{\sqrt{Q_{x,k}^2 + P_{x,k}^2}} \in [0, 1[$ is the power factor of k-th converter, $\alpha = \max\left\{\frac{\mu^2 v_{\mathrm{dc}}^{*2}}{16\,R}, \frac{\mu\, v_{\mathrm{dc}}^{*2}}{4\sqrt{Y^{-2}-1}}\right\}$, $Y = \frac{1}{2}\mu v_{\mathrm{dc}}^* L^{-1} \sup_\zeta \|(j\zeta\mathbf{I} - F)^{-1}\|_2$, where $Y < 1$. Additionally, assume that

$$\frac{\frac{\mu}{2}(1 + \eta\, C_{\mathrm{dc}} v_{\mathrm{dc}}^* Q_{x,k}^{-1})}{\sqrt{\frac{4}{v_{\mathrm{dc}}^{*2}}(Y^{-2} - 1) - \frac{1}{4}\mu^2 v_{\mathrm{dc}}^{*2}\, Q_{x,k}^{-2}}} < K_p, \quad k = 1, \ldots, n. \tag{25}$$

Next, we provide the main result of this section.

Lemma V.5: Consider the linearized closed-loop multi-converter model (22). Under Condition V.4, the subspace span$\{v(z^*)\}$ is asymptotically stable.

Proof.: Since $v(z^*) \in \ker(J_f(z^*))$, Assumption 3 is satisfied. If (24) is true, then $r^\top(\gamma_k^*)J^\top i_k^* > 0$, for all $k = 1, \ldots n$, the submatrix A_{11} is Hurwitz and hence Assumption 2 is also valid.

Next, we verify Assumption 4. First, the matrix P_1 can be identified from specification ①with $\mathcal{Q}_1 = \mathbf{I}$ by the following expressions:

$$P_{11} = \frac{1}{\eta}\left[\frac{1}{2}K_p(\nabla^2 U(\gamma^*))^{-1} + \frac{\nabla^2 U(\gamma^*)}{2K_p} \times (\mathbf{I} + \eta C_{\mathrm{dc}}(\nabla^2 U(\gamma^*))^{-1})\right]$$

$$P_{12} = P_{12}^\top = \frac{1}{2}(\nabla^2 U(\gamma^*))^{-1} C_{\mathrm{dc}}$$

$$P_{22} = \frac{C_{\mathrm{dc}}}{2K_p}\left(\mathbf{I} + \eta C_{\mathrm{dc}}\,(\nabla^2 U(\gamma^*))^{-1}\right).$$

The feasibility of specification ②with the positive semidefinite matrix $\mathcal{Q}_2 = \mathbf{I} - \frac{v_2^* v_2^{*\top}}{v_2^{*\top} v_2^*}$ is given by

$$P_2\, A_{21} A_{21}{}^\top P_2 + P_2 F + F^\top P_2 + NN^\top + \mathcal{Q}_2 = 0 \tag{27}$$

where $F = A_{22} + A_{21}P_1A_{12}$ and $N = A_{12}^\top P_1$. If Assumption 4 is satisfied, then there exists a positive definite matrix P_2 that satisfies $\mathcal{H}_\infty-$ARE in (27).

Next, we find sufficient conditions, for which F satisfies the Lyapunov equation $P_F F + F^\top P_F = -\mathcal{Q}_F$. We choose P_F and $\mathcal{Q}_F$ to be block-diagonal matrices

$$P_F = \begin{bmatrix} L & 0 & 0 \\ 0 & C & 0 \\ 0 & 0 & L_\ell \end{bmatrix}, \quad \mathcal{Q}_F = \begin{bmatrix} \Gamma & 0 & 0 \\ 0 & 2G\,\mathbf{I} & 0 \\ 0 & 0 & 2R_\ell\mathbf{I} \end{bmatrix}$$

with

$$\Gamma = 2R\,\mathbf{I} + C_{\mathrm{dc}}^{-1}\left(\Xi(\gamma^*)P_{12}\Lambda(\gamma^*)^\top + \Lambda(\gamma^*)P_{12}\Xi(\gamma^*)^\top\right) + 2C_{\mathrm{dc}}^{-1}\left(\Lambda(\gamma^*)P_{22}\Lambda(\gamma^*)^\top\right)$$

being itself block-diagonal. Aside from Γ, all diagonal blocks of P_F and $\mathcal{Q}_F$ are positive definite. We evaluate the block-diagonal matrix Γ for positive definiteness by exploring its two-by-two block diagonals, where trace and determinant of each block are positive under

$$Q_{x,k}^* = \frac{1}{2}v_{\mathrm{dc}}^*\mu(r(\gamma_k^*))^\top J^\top i_k^* > \frac{\mu^2 v_{\mathrm{dc}}^{*2}}{16\,R}.$$

Furthermore, we impose $\|\mathcal{G}\|_\infty < 1$, by equivalently setting $\sup_{\zeta\in\mathbb{R}} \|\mathcal{C}\,(j\zeta\mathbf{I} - F)^{-1}B\|_2 < 1$, where

$$\mathcal{C} = \left(A_{12}^\top P_1^\top P_1 A_{12} + \mathbf{I} - \frac{(\mathbf{J}x^*)(\mathbf{J}x^*)^\top}{(\mathbf{J}x^*)^\top(\mathbf{J}x^*)}\right)^{1/2}, \quad B = A_{21}.$$

It is sufficient to consider $\|\mathcal{C}\|_2^2 < (\sup_{\zeta\in\mathbb{R}} \|(j\zeta\mathbf{I} - F)^{-1}\|_2\|B\|_2)^{-2}$. Using the triangle inequality for the induced two-norm, we arrive at $\|\mathcal{C}\|_2^2 \leq \|A_{12}^\top P_1^\top P_1 A_{12}\|_2 + \|\mathcal{Q}_2\|_2$. Since $\|\mathcal{Q}_2\|_2 = 1$, we consider instead

$$\|A_{12}^\top P_1^\top P_1 A_{12}\|_2 \leq (\sup_\zeta \|(j\zeta I - F)^{-1}\|_2\|B\|_2)^{-2} - 1.$$

Additionally, it holds that

$$\|B\|_2^2 = \|A_{21}\|_2^2 = L^{-2}\| \begin{bmatrix} \Xi^\top\Xi & \Xi^\top\Lambda \\ \Lambda^\top\Xi & \Lambda^\top\Lambda \end{bmatrix} \|_2 =$$

$$L^{-2}\| \begin{bmatrix} \Xi^\top\Xi & 0 \\ 0 & \Lambda^\top\Lambda \end{bmatrix} \|_2 = \left(\frac{1}{2}\mu v_{\rm dc}^*\right)^2 L^{-2}$$

where the last equality follows from $v_{\rm dc}^* \geq 1$. Define $Y = \frac{1}{2}\mu v_{\rm dc}^* \sup_\zeta \|(j\,\zeta\mathbf{I} - F)^{-1}\|_2\, L^{-1}$. For $Y < 1$, straightforward calculations show that

$$\|A_{12}^\top P_1^\top P_1 A_{12}\|_2 = \overline{\sigma}(C_{\rm dc}^{-2}\Lambda(\gamma^*)(P_{12}^2 + P_{22}^2)\Lambda(\gamma^*)^\top)$$

$$= \max_{k=1,\ldots,n} d_k \overline{\sigma}(r(\gamma_k^*)r^\top(\gamma_k^*))) < \frac{4}{v_{\rm dc}^{*2}}(Y^{-2} - 1)$$

with

$$d_k = (r_k^\top(\gamma_k^*)J^\top i_k^*)^{-2} + \frac{1}{4K_p^2}\left(1 + \eta C_{\rm dc}(\frac{1}{2}\mu r^\top(\gamma_k^*)J^\top i_k^*)^{-1}\right)^2.$$

Under $4/v_{\rm dc}^{*2}\,(Y^{-2} - 1) - \max_{k=1,\ldots,n}(r_k^\top(\gamma_k^*)J^\top i_k^*)^{-2} > 0$, we solve for the gain K_p with $\overline{\sigma}(r(\gamma_k^*)r^\top(\gamma_k^*)) = 1,\ k = 1,\ldots,n$, to find,

$$\sqrt{\frac{\max\limits_{k=1,\ldots,n} \frac{\mu^2}{4}(1 + \eta C_{\rm dc}(\frac{1}{2}\mu\, r^\top(\gamma_k^*)\, J^\top i_k^*)^{-1})^2}{\frac{4}{v_{\rm dc}^{*2}}(Y^{-2} - 1) - \max\limits_{k=1,\ldots,n}(r^\top(\gamma_k^*)\, J^\top i_k^*)^{-2}}} < K_p.$$

This can be simplified into (25). The condition

$$4/v_{\rm dc}^{*2}\,(Y^{-2} - 1) - \max_{k=1,\ldots,n}(r_k^\top(\gamma_k^*)J^\top i_k^*)^{-2} > 0$$

can be written as $Q_{x,k}^2 > \frac{\mu^2 v_{\rm dc}^{*4}}{16(Y^{-2}-1)}$ under the assumption that $Y < 1$ and we deduce that

$$\max\left\{\frac{\mu^2 v_{\rm dc}^{*2}}{16\,R}, \frac{\mu\, v_{\rm dc}^{*2}}{4\sqrt{Y^{-2} - 1}}\right\} < Q_{x,k}.$$

From the definition of the power factor $\cos(\phi_k) = \frac{P_{x,k}}{\sqrt{Q_{x,k}^2 + P_{x,k}^2}}$, we arrive at (24). In summary, we arrive at (25) and (24). By applying Theorem IV.3, we deduce that span$\{v(x^*)\}$ is asymptotically stable for the linearized system (22). ■

C. Results Contextualization

Generally speaking, (24) and (25) can be regarded as a requirements on the ac and dc side, respectively. Both of them are explicit and sufficient for asymptotic stability.

Condition (24) connects the efficiency of the converter given by the power factor that defines the amount of current producing useful work to the lower bound $\alpha > 0$. From (24), the power factor approaches 1, as $\alpha \to 0$.

If $\max\{\frac{\mu^2 v_{\rm dc}^{*2}}{16\,R}, \frac{\mu v_{\rm dc}^{*2}}{4\sqrt{Y^{-2}-1}}\} = \frac{\mu^2 v_{\rm dc}^{*2}}{16\,R}$, then (24) depends on the converter's resistance R, modulation amplitude μ, nominal dc voltage $v_{\rm dc}^*$, and the steady-state current i^*. This is a known practical stability condition [23]. In fact from (24), sufficient resistive damping is often enforced by *virtual impedance control,* which makes $\alpha \to 0$.

If $\max\{\frac{\mu^2 v_{\rm dc}^{*2}}{16\,R}, \frac{\mu v_{\rm dc}^{*2}}{4\sqrt{Y^{-2}-1}}\} = \frac{\mu v_{\rm dc}^{*2}}{4\sqrt{Y^{-2}-1}}$, then we can again deploy $\mathcal{H}_\infty$ control to make $\|G_{\rm ac}\|_\infty$ arbitrarily small and thus $\alpha \to 0$. We note that the ac side feedback control is crucial to achieve desired steady states for our power system model (4). This can be implemented, e.g., via outer loops that take ac measurements and use the classical vector control architecture for the regulation of the inductance current and the output capacitor voltage; see, e.g., [24].

That $Y < 1$ translates into the requirement

$$\|G_{\rm ac}\|_\infty < \beta,\ \beta = \frac{2\,L}{\mu v_{\rm dc}^*}$$

where $G_{\rm ac}(j\zeta) = (j\zeta\mathbf{I} - F)^{-1}$ asks for $\mathcal{L}_2$ gain from the disturbances on the ac side to ac signals to be less than β. This can be achieved via $\mathcal{H}_\infty$ control; see [25].

Condition (25) depends on the steady-state angles γ^* and the converter and network parameters and asks for damping as for other stability conditions obtained in the literature on the study of synchronous machines [3], [4]. Note that the smaller is the *synchronization* gain $\eta > 0$, the larger is the operating range of the dc damping gain K_p.

For more general settings with heterogeneous converters and transmission lines parameters, our stability analysis can be applied and analogous sufficient and explicit conditions to (24) and (25) can be derived.

TABLE I
PARAMETER VALUES OF THE CONVERTERS AND THE RL LINES (IN S.I)

	$C_i,\ i = \{1,2,3\}$	RL Lines
i_{dc}^*	16.5	–
v_{dc}^*	1000	–
C_{dc}	10^{-3}	–
G_{dc}	10^{-5}	–
K_P	0.099	–
η	0.0003142	–
μ	0.33	–
L	$5\cdot10^{-4}$	–
C	10^{-5}	–
G	0.1	–
R	0.2	–
R_ℓ	–	0.2
L_ℓ	–	$5\cdot10^{-5}$

VI. SIMULATIONS

The goal of this section is to assess the asymptotic stability of the trajectories of the nonlinear power system (4) in Theorem IV.3 locally, i.e., by numerically finding an estimate of the region of attraction $\mathcal{N}$ for a given $z^* = [\gamma^{*\top}, 0^\top, v_c^{*\top}, i_\ell^{*\top}]^\top$. Let us consider three identical dc/ac converters in closed-loop with the matching control depicted in Fig. 2 and connected via three identical resistive and inductive lines, as in (4) and connected to

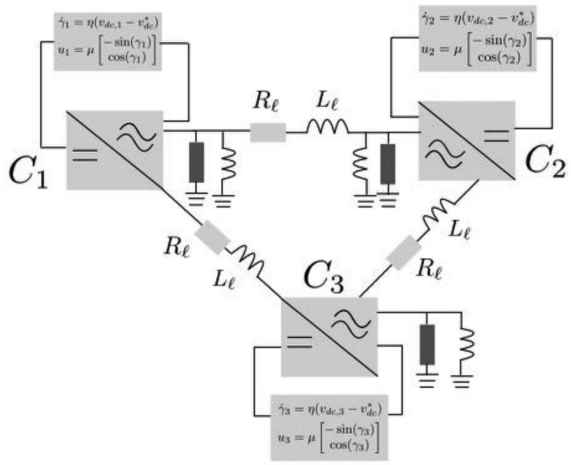

Fig. 2. Three-converter setup with dynamics described by (4), consisting of identical three-phase converters C_1, C_2, and C_3 in closed-loop with the matching control and connected via identical RL lines. The internal dynamics of each converter are modeled as in Fig. 1.

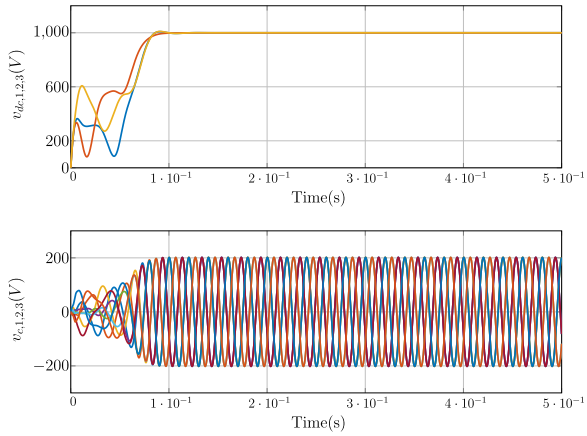

Fig. 4. Synchronization of dc capacitor voltages corresponds to frequency synchronization at the desired value. Hereby, the angles are initialized at $(-6, -2, -13.15)$ (in rad) and belong to the region estimated in Fig. 3. The ac capacitor voltage v_c (resulting from transforming v into $abc-$frame using inverse Park followed by inverse Clarke transformation) converges to a sinusoidal steady state v_c^*.

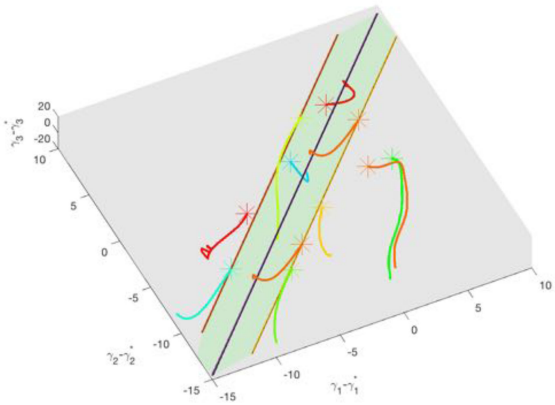

Fig. 3. Representation of the region of attraction $\mathcal{N}$ and the frequency synchronous steady state set $\mathcal{S}(z^*)$ restricted to $(\gamma_1 - \gamma_1^*, \gamma_2 - \gamma_2^*, \gamma_3 - \gamma_3^*)-$space of the three dc/ac converter angles and convergence of the sample angle trajectories of (4) to the subspace $\mathbb{1}_3$. The depicted region is obtained from varying the initial angles, while keeping the remaining initial states fixed. A sample of angles deviations initialized within the green area and denoted by stars converge toward the stable set, while some angle trajectories initialized outside the estimated region are divergent. The green area is defined by $d(\gamma(0), \text{span}\{\mathbb{1}_3\}) = \| \left(\mathbf{I} - \frac{\mathbb{1}_3 \mathbb{1}_3^\top}{\mathbb{1}_3^\top \mathbb{1}_3} \right) \gamma(0) \|_2 = 3.1$ (in rad), where $\gamma(0)$ is the angle vector initialized on the boundary of $\mathcal{N}$. All the angles are represented in rad.

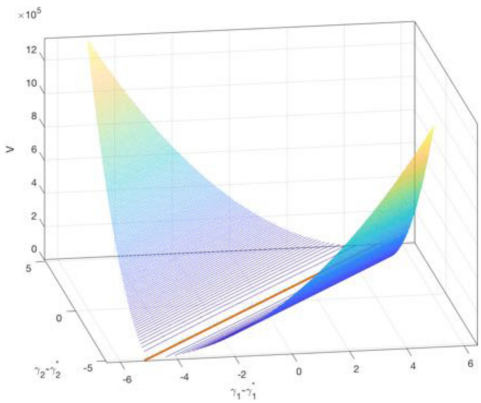

Fig. 5. $3D-$representation of the Lyapunov function $V(x)$ in (19) for *two* dc/ac converters in closed-loop with the matching control and connected via an RL line in (3) after a projection into $(\gamma_1 - \gamma_1^*, \gamma_2 - \gamma_2^*)$ space for $P > 0$ as in (23) and the subspace spanning $v(x^*)$. The parameter values can be found in Table I.

an inductive and resistive load to ground. Table I summaries the converter parameters and their controls (in S.I.).

First, we start by verifying the parametric conditions established in Condition V.4 via (24) and (25). We tune the filter resistance $R > 0$ (e.g., using virtual impedance control) and choose the dc side gain $K_p > 0$ so that (24) and (25) are satisfied, respectively.

Second, we numerically estimate the region of attraction $\mathcal{N}$ in $\gamma-$space by initializing sample trajectories of the angles depicted in Fig. 2 at various locations and illustrate the evolution of the angle trajectories of (4) to estimate a projection of $\mathcal{N}$ into the angle space. As predicted by Theorem IV.3, we observe that the set $\mathcal{S}(z^*)$ restricted to the angles (relative to their steady state) space, and represented by $\text{span}\{\mathbb{1}_3\}$ is asymptotically stable for the sampled angle trajectories of (4).

Fig. 3 depicts a projection onto $(\gamma_1, \gamma_2, \gamma_3)-$space of the estimate of $\mathcal{N}$ (in rad and relative to their respective steady-state values). The convergence of angle trajectories to the subspace $\mathbb{1}_3$ is guaranteed for initial conditions at distance

$$d(\gamma(0), \text{span}\{\mathbb{1}_3\}) = \| \left(\mathbf{I} - \frac{\mathbb{1}_3 \mathbb{1}_3^\top}{\mathbb{1}_3^\top \mathbb{1}_3} \right) \gamma(0) \|_2 = 3.1 (\text{in rad})$$

resulting from varying the initial angles $\gamma(0)$, while keeping the remaining initial states fixed. In particular, dc voltages and ac currents are also initialized close to their steady-state values, as shown in Fig. 4. Our simulations show that the dc capacitor voltage v_{dc} in Fig. 4 and the ac output capacitor voltage v_c in $abc-$frame (resulting from transforming v into $abc-$frame using inverse Park transformation followed by inverse Clarke transformation) converge to their respective steady-state values. This validates our theoretical results from Section IV.

For completeness, we also illustrate a projection of the level sets of the Lyapunov function (19) of an example network consisting of *two* dc/ac converters connected via one *RL* line (for more details see [26]) with system dynamics (4) into $(\gamma_1, \gamma_2)-$space (in rad and relative to their respective steady-state values) in Fig. 5. The parameter values can be taken from Table I. The vector $v(z^*) = [\, v_1^\top(z^*)\ v_2^\top(z^*)\,]^\top \in \ker(J_f(z^*))$, is given by

$$v_1(z^*) = \big[\, 0.043,\ 0.043,\ 0,\ 0 \,\big]^\top$$

and

$$v_2(z^*) = [\, -0.0033\ -0.0023\ -0.0033\ -0.0023 \\ -0.7034\ -0.0108\ -0.7034\ -0.0108\ 0\ 0\,].$$

For a positive definite matrix P given by (23), the function $V(x)$ takes positive values everywhere and is zero on the subspace spanned by $v(z^*)$ and given by Fig. 5.

VII. Conclusion

We investigated the characteristics of a high-order steady-state manifold of a multi-converter power system by exploiting the symmetry of the vector field. We studied local asymptotic stability of the steady-state set as a direct application of the center manifold theory and provided an operating range for the control gains and converter parameters. Future directions include finding better estimates of the region of attraction using advanced numerical methods and large-scale simulations of the power system dynamics.

Acknowledgment

The authors would like to thank Florian Dörfler, Anders Rantzer, Richard Pates, and Mohammed Deghat for the insightful and important discussions.

References

[1] P. Prachi, "How inexpensive must energy storage be for utilities to switch to 100 percent renewables?," 2019. [Online]. Available: https://spectrum.ieee.org/what-energy-storage-would-have-to-cost-for-a-renewable-grid

[2] P. Kundur, N. J. Balu, and M. G. Lauby, *Power System Stability and Control*, vol. 7. New York, NY, USA: McGraw-Hill, 1994.

[3] F. Dörfler and F. Bullo, "Synchronization and transient stability in power networks and nonuniform Kuramoto oscillators," *SIAM J. Control Optim.*, vol. 50, no. 3, pp. 1616–1642, 2012.

[4] C. Arghir, T. Jouini, and F. Dörfler, "Grid-forming control for power converters based on matching of synchronous machines," *Automatica*, vol. 95, pp. 273–282, Sep. 2018. [Online]. Available: https://doi.org/10.1016/j.automatica.2018.05.037

[5] A. Sarlette, "Geometry and symmetries in coordination control," Ph.D. dissertation, Univ. Liège, Liège, Belgium, 2009. [Online]. Available: https://hdl.handle.net/2268/9544

[6] J. Schiffer, D. Efimov, and R. Ortega, "Global synchronization analysis of droop-controlled microgridsa multivariable cell structure approach," *Automatica*, vol. 109, Nov. 2019, Art. no. 108550. [Online]. Available: https://doi.org/10.1016/j.automatica.2019.108550

[7] E. Tegling, B. Bamieh, and D. F. Gayme, "The price of synchrony: Evaluating the resistive losses in synchronizing power networks," *IEEE Trans. Control Netw. Syst.*, vol. 2, no. 3, pp. 254–266, Sep. 2015.

[8] S. Y. Caliskan and P. Tabuada, "Compositional transient stability analysis of multimachine power networks," *IEEE Trans. Control Netw. Syst.*, vol. 1, no. 1, pp. 4–14, Mar. 2014.

[9] B. B. Johnson, S. V. Dhople, A. O. Hamadeh, and P. T. Krein, "Synchronization of parallel single-phase inverters with virtual oscillator control," *IEEE Trans. Power Electron.*, vol. 29, no. 11, pp. 6124–6138, Nov. 2014.

[10] H. K. Khalil, *Nonlinear System*, vol. 3. Upper Saddle River, NJ, USA: Prentice-Hall, 2002.

[11] T. L. Vu and K. Turitsyn, "Lyapunov functions family approach to transient stability assessment," *IEEE Trans. Power Syst.*, vol. 31, no. 2, pp. 1269–1277, Mar. 2016.

[12] T. Jouini and Z. Sun, "Fully decentralized conditions for local convergence of DC/AC converter network based on matching control," in *Proc. 59th IEEE Conf. Decis. Control*, 2020, pp. 836–841.

[13] S. Wiggins, *Introduction to Applied Nonlinear Dynamical Systems and Chaos*, vol. 2. Berlin, Germany: Springer, 1990.

[14] B. Wittig, W.-T. Franke, and F. Fuchs, "Design and analysis of a DC/DC/AC three phase solar converter with minimized DC link capacitance," in *Proc. 13th Eur. Conf. Power Electron. Appl.*, 2009, pp. 1–9.

[15] J. W. Simpson-Porco, F. Dörfler, and F. Bullo, "Synchronization and power sharing for droop-controlled inverters in islanded microgrids," *Automatica*, vol. 49, no. 9, pp. 2603–2611, Sep. 2013. [Online]. Available: https://doi.org/10.1016/j.automatica.2013.05.018

[16] A. Isidori and C. Byrnes, "Output regulation of nonlinear systems," *IEEE Trans. Autom. Control*, vol. 35, no. 2, pp. 131–140, Feb. 1990.

[17] J. Carr, *Applications of Centre Manifold Theory*, vol. 35. Berlin, Germany: Springer, 2012.

[18] D. Angeli, "An almost global notion of input-to-state stability," *IEEE Trans. Autom. Control*, vol. 49, no. 6, pp. 866–874, Jun. 2004.

[19] J. Willems, "Comments on a general Liapunov function for multimachine power systems with transfer conductances," *Int. J. Control*, vol. 23, no. 1, pp. 147–148, 1976.

[20] H.-D. Chiang, "Study of the existence of energy functions for power systems with losses," *IEEE Trans. Circuits Syst.*, vol. 36, no. 11, pp. 1423–1429, Nov. 1989.

[21] Y. Lin, E. D. Sontag, and Y. Wang, "A smooth converse lyapunov theorem for robust stability," *SIAM J. Control Optim.*, vol. 34, no. 1, pp. 124–160, Jan. 1996. [Online]. Available: https://doi.org/10.1137/s0363012993259981

[22] C. Scherer, "Theory of robust control," Delft Univ. Technol., Delft, The Netherlands, pp. 1–160, 2001.

[23] X. Wang, Y. W. Li, F. Blaabjerg, and P. C. Loh, "Virtual-impedance-based control for voltage-source and current-source converters," *IEEE Trans. Power Electron.*, vol. 30, no. 12, pp. 7019–7037, Dec. 2015.

[24] S. D'Arco, J. A. Suul, and O. B. Fosso, "A virtual synchronous machine implementation for distributed control of power converters in smartgrids," *Elect. Power Syst. Res.*, vol. 122, pp. 180–197, 2015.

[25] K. Zhou *et al.*, *Robust and Optimal Control*, vol. 40. Upper Saddle River, NJ, USA: Prentice-Hall, 1996.

[26] T. Jouini and F. Dörfler, "Local synchronization of two DC/AC converters via matching control," in *Proc. 18th Eur. Control Conf.*, 2019, pp. 2996–3001.

Taouba Jouini (Member, IEEE) received the B.Sc. and M.Sc. degrees in cybernetics engineering from the University of Stuttgart, Stuttgart, Germany, in 2013 and 2016, respectively. She is currently working toward the Ph.D. degree in automatic control at LTH, Lund University, Lund, Sweden.

She was a Graduate Research Assistant with the Automatic Control Laboratory (IfA) at ETH Zurich from 2016 to 2019. Her research interests are centered around modeling and control of networked and multiagent systems with application to power system networks.

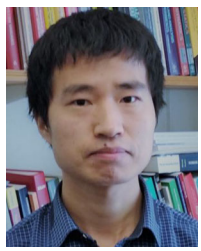

Zhiyong Sun (Member, IEEE) received the Ph.D. degree in control engineering from The Australian National University (ANU), Canberra ACT, Australia, in 2017.

He was a Research Fellow/Lecturer with the Research School of Engineering, ANU, from 2017 to 2018. From 2018 to 2020, he worked as a Postdoctoral Researcher with the Department of Automatic Control, Lund University, Lund, Sweden. Since January 2020, he has been with Eindhoven University of Technology (TU/e), the Netherlands, as an Assistant Professor. His research interests include multiagent systems, control of autonomous formations, and distributed optimization.